Arabian Journal of Geosciences,
13, *(20)*, 1055, 13 pp., 2020.

2ND CAJG 2019

Tsunami simulations along the Eastern African coast from mega-earthquake sources in the Indian Ocean

Amir Salaree[1,2] · **Emile A. Okal**[1]

Received: 21 April 2020 / Accepted: 20 August 2020

Abstract

The catastrophic 2004 Indonesian tsunami reached the shores of Eastern Africa, where it affected at least 12 countries and caused several hundred casualties, principally in Somalia. Significant variations in run-up were documented by various post-tsunami surveys (note that the latter remain incomplete, especially in Southern Tanzania and Mozambique). In a previous study, Okal et al. (S Afr J Geology 112:343–358, 2009) suggested that these variations could depend on the precise location of the tsunami sources, as a result of the combined effect of source directivity and refraction by irregular bathymetry. In this context, we present the results of a significantly enhanced study, which considers a total of twelve potential sites of mega-earthquakes, along both the Sunda Arc, and the Makran subduction zone. Numerical simulations are carried out at a total of 35 virtual gauges, spanning the East African coast from Socotra in the North to Port Elizabeth in the South, as well as adjoining islands (Madagascar, Comoros, Mascarenes), the Gulf of Aden, and distant islands in the far Southern Indian Ocean, from Amsterdam to Prince Edward. We conclude that at many locations, in particular in Mozambique, South Africa, Madagascar, and the Mascarenes, the 2004 tsunami (which to a large extent awakened the awareness of the continent to tsunami danger) may not have represented a worst case scenario. For tsunamis originating in the Makran, amplitudes larger than in 1945 require the simultaneous rupture of several blocks of the plate boundary, a scenario which, although not impossible, remains at this stage speculative.

Keywords Tsunami · Indian Ocean · East Africa

Introduction and background

The Sumatra-Andaman tsunami of 26 December 2004 was the first in modern history to export death and destruction across the Indian Ocean Basin, resulting in more than 45,000 casualties in India and Sri Lanka alone. Farther out, it affected the coastlines of Eastern Africa, where it caused an additional ~300 casualties, principally in Somalia, but also all the way to South Africa where two people drowned at beaches near Port Elizabeth (Rabinovich and Thomson 2007). In the following months and years, a number of extensive field surveys mapped run-up ranging up to 9 m in Somalia, 6.9 m in Grande Comore, and 5 m at the Southern tip of Madagascar (Fritz and Borrero 2006; Fritz and Okal 2008; Okal et al. 2006a, b, c, 2009; Weiss and Bahlburg 2006); note however a significant gap in surveying in central and Southern Somalia, in Southern Tanzania, and along all the coast of Mozambique.

The 2004 disaster served as a tragic wake-up call to raise awareness of tsunami hazard among coastal populations of the Indian Ocean Basin, and in particular in East Africa. In its immediate wake, the Pacific Tsunami Warning Center in Hawaii and the Japan Meteorological Agency were given temporary responsibility for the issuance of warnings in the Indian Ocean (Anonymous 2005), a function now transferred to regional outfits, following the development of adequate tsunami warning centers in a growing number of countries, including, e.g., Australia, Indonesia, India, and Oman (Bernard and Titov 2015).

This paper was selected from the 2nd Conference of the Arabian Journal of Geosciences (CAJG), Tunisia 2019

Communicated by: Santanu Banerjee

✉ Emile A. Okal
emile@earth.northwestern.edu

[1] Department of Earth and Planetary Sciences, Northwestern University, Evanston, IL 60208, USA

[2] Department of Earth and Environmental Sciences, University of Michigan, Ann Arbor, MI 48109, USA

In a previous study, Okal et al. (2009; hereafter Paper I) used numerical simulations to investigate a number of credible scenarios for future large Indonesian tsunamis impacting the Western Indian Ocean shorelines. Those included both events documented in the seismic record, such as the 2007 Bengkulu earthquake (Borrero et al. 2009), or reconstructed from the study of coral uplift, such as the 1833 Mentawai Islands event (Zachariasen et al. 1999), as well as a model of the widely expected mega-event at the Padang gap (McCloskey et al. 2010), and also a more speculative source involving the southern section of the Sumatra subduction zone. Paper I concluded that local effects were responsible for significant lateral variations of run-up, which in turn meant that the 2004 event may not constitute a worst-case scenario at several locations along the coastlines of East Africa and its neighboring islands.

In this context, we present here an update of the study in Paper I, which is enhanced in several respects. First, we nearly double the number of virtual gauges, from 19 to 35 (Fig. 1), by targeting additional shorelines in Tanzania and Northern Mozambique, as well as in the Gulf of Aden. We also include gauges near five isolated islands of the Southern Indian Ocean, all of which except St. Paul hold permanently manned scientific research stations. Second, we fine-tune the position of all virtual gauges to ensure (with one exception) a commonality of water depth, chosen as 1000 m, for all locations. While final tsunami amplitudes at shorelines are controlled by the interaction of the wave with local bathymetry, as well as the exact site response of coastal features such as bays and harbors, these effects depend critically on small scale bathymetry, often unavailable or proprietary in foreign jurisdictions. Under those conditions, and for sources of comparable sizes (hence characterized by similar wavelengths (Rabinovich 1997)), arriving at comparable azimuths, simulated values in deep water represent an acceptable compromise allowing the meaningful comparison of relative amplitudes at different gauges, irrespective of the effect of shoaling. The exception is gauge 101, near Djibouti in the Gulf of Aden, which is located at a depth of 856 m, this difference resulting in an amplification of only 4% under Green's (1838) law.

Finally, we add sources in the Makran subduction zone, the only other region with known earthquakes having generated large tsunamis in the Indian Ocean Basin.

We emphasize here the deterministic character of our investigation: As in Paper I and in previous studies such as Okal and Synolakis (2008), we consider a number of earthquake scenarios without attempting to formally quantify the likelihood of their occurrence. Reliable earthquake catalogues for Sumatra may be tentatively available for at most a few centuries, while paleotsunami investigations initiated in the wake of the 2004 disaster have pointed out to recurrence times as large as ~1000 years (Jankaew et al. 2008), recently supported by sedimentological investigations in India (Rajendran et al. 2006) and Tanzania (Maselli et al. 2020). With the additional caveat of the probable irregularity in fault fragmentation (Ando 1975), we find it difficult to define a possible recurrence time for an event such as the 1833 Mentawai earthquake, whose tsunami was not beamed at densely populated areas such as India. In this context, our deterministic approach, which emphasizes *relative* tsunami amplitudes for selected location and sources, appears complementary to probabilistic hazard assessment studies such as Davies et al. (2018), and in particular for the Indian Ocean, Burbidge et al. (2009). However, when possible and appropriate, we will discuss our results in the context of those studies.

Hydrodynamic simulations

Earthquake sources

We use sources located at both the Sumatra and Makran Trenches, with all relevant parameters summarized in Table 1, which reproduces and expands a similar table in Paper I. Sumatra sources are identical to those used in Paper I. Source **S.I** models the 2004 event as a composite rupture. Source **S.II** uses Okal and Synolakis' (2008) model of the 1833 earthquake, based on the work of Zachariasen et al. (1999) and Natawidjaja et al. (2006). Source **S.III** models the main 2007 Bengkulu earthquake, using Borrero et al.'s (2009) simple source. Source **S.IV** releases the strain left over on the 1797 and 1833 ruptures after the 2007 Bengkulu event, as detailed in Okal and Synolakis (2008); it is representative of the widely expected Padang earthquake which should close that seismic gap in the next decades (McCloskey et al. 2010). Finally, source **S.V** is similar to **S.IV**, but extends South towards the Sunda Straits, and reproduces Okal and Synolakis' (2008) speculative model 2*a*.

In the case of the Makran sources, we use the earthquake of 27 November 1945 as source **M.B**. This event generated a devastating tsunami, with a large number of casualties in present-day Pakistan (Pendse 1948). Its mechanism and long-period moment are taken from Okal et al.'s (2015) inversion using the PDFM technique (Reymond and Okal 2000). Historical records (Oldham 1893; Ambraseys and Melville 1982) suggest the occurrence of tsunamigenic earthquakes on either side of the 1945 rupture, in 1851 (and possibly 1864) to the West, and in 1765 to the East. Following Okal and Synolakis (2008), we use such scenarios as models **M.A** and **M.C**, respectively. In the absence of detailed information about the source of these events, we assign them sizes and mechanisms similar to

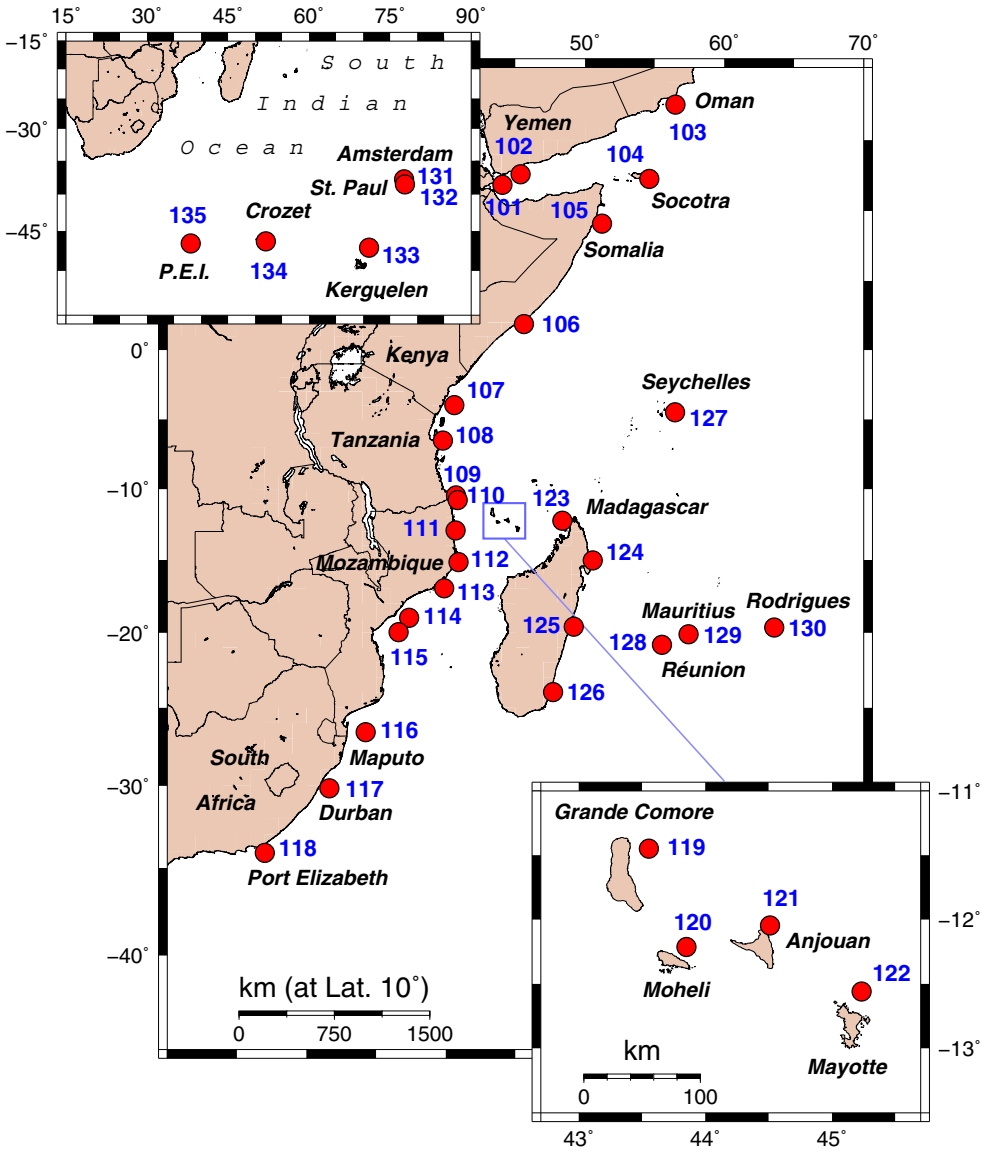

Fig. 1 Map of the 35 virtual gauges used in this study. The numbers are keyed to the indices listed in Table 1. The lower-right inset zooms on the Comoro Archipelago shown as the gray box on the main map; the upper-left one shows the five gauges located next to the Southern islands of the Indian Ocean

those of the 1945 shock (model **M.B**), with the exception of the azimuth ϕ which we take as 281° in model **M.A**, in order to reflect the change in morphology of the coastline.

We then use the concept of fault fragmentation along a subduction zone to build three additional models in which two or more of the three blocks (A, B, C) rupture simultaneously. This concept, introduced by Ando (1975) in the case of the Nankai Trough, has later been confirmed in several other subduction systems, such as the Kuriles (Nanayama et al. 2003), Cascadia (Kelsey et al. 2005), and Southern Chile (Cisternas et al. 2005). Here, we consider model **M.D** as a combined rupture of A and B, model **M.E** as that of B and C, and finally model **M.F** as the full rupture of all three segments A, B, and C.

Finally, we note that the exact tectonic regime of the Western part of the Makran subduction zone (West of source **M.A**) remains controversial. In the absence of firmly documented evidence for large-scale seismicity, the convergence between Arabia and Eurasia (in excess of that taken up by onland orogeny) could be accommodated through either aseismic slip, or mega-thrust events recurring on a time scale of 1000 years or more, so that none would be known in the available historical record (Mokhtari et al. 2008; Rajendran et al. 2013). This situation is comparable with that which prevailed in Cascadia prior to the identification of the large 1700 earthquake (White and Klitgord 1976). Based on this remark, Okal and Synolakis (2008) considered the possibility of a mega-thrust scenario prolonging model **M.F** ∼450 km to the West (their model 6), with a total moment of 4.7×10^{29} dyn*cm, comparable with that of the 2011 Tohoku earthquake. We incorporate this model as scenario **M.G**, while stressing that it represents a very improbable situation combining several assumptions, all of which highly speculative: (i) that the

Table 1 Parameters of the sources used in the numerical simulations

Number	Source	Centroid		Fault parameters			Moment	Focal mechanism		
		(° N)	(° E)	Length L (km)	Width W (km)	Slip Δu (m)	(10^{29} dyn*cm)	ϕ (°)	δ (°)	λ (°)
Sumatra sources										
S.I.a	2004,a	3.3	94.6	382	150	11.5	3.2	318	6.4	94
S.I.b	2004,b	7.0	93.8	818	150	12.4	7.3	355	7	109
S.I	Sumatra-Andaman 2004			1200	150		10.5			
S.II	Mentawai 1833	−3.0	99.7	550	175	13	6.0	322	12	90
S.III	Bengkulu 2007	−4.4	101.6	190	95	5.6	0.5	329	8	100
S.IV	1833 post-2007	−3.7	100.6	350	175	6.0	1.9	322	12	90
S.V	IV + South	−4.25	100.7	900	175	8.0	6.0	322	12	90
Makran sources										
M.A	1851	24.85	62.1	157	78	4.62	0.28	281	9	89
M.B	1945	24.86	63.55	157	78	4.62	0.28	261	9	89
M.C	1765	25.1	65.1	157	78	4.62	0.28	261	9	89
M.D	A + B						0.56			
M.E	B + C						0.56			
M.F	A +B + C						0.84			
M.G	F + West						4.70			

Western Makran is a coupled subduction zone, when the only evidence of a major earthquake is a poorly constrained shock in 1483 (Musson 2009); (ii) that a single mega-event in the form of Okal and Synolakis' (2008) model 6 could rupture the entire Makran coast, when the cross-cutting strike-slip Sonne Fault may interrupt the continuity of the subduction system (Kukowski et al. 2000); and (iii) that the slip on such a rupture would grow according to seismic similitude laws. That speculative nature will be emphasized when discussing our results.

Simulation algorithm

Our simulations use the MOST algorithm (Titov and Synolakis 1998; Titov et al. 2016), which solves the full non-linear equations of hydrodynamics under the shallow-water approximation, by finite differences and using the method of alternate steps (Godunov 1959). MOST has been extensively validated through comparisons with laboratory and field data, per standard international protocols (Synolakis et al. 2008); full details can be found in Synolakis (2003).

As initial conditions for the vertical displacements of the sea surface, $\eta\,(t = 0_+)$, we use the field of static deformations resulting from the seismic dislocation, computed through the algorithm of Mansinha and Smylie (1971) in the geometry of a homogeneous half-space. This approximation is appropriate as the rise time of an earthquake is always much shorter than the characteristic time needed by a tsunami wave to flush the displaced water out of the generation area (e.g., Saito and Furumura 2009; Derakhti et al. 2019). For the composite mechanism of source **S.I**, we simply superimpose the fields of deformation of the two individual subevents.

The simulations use the 2-arcmin grid ETOPO2 (Anonymous 2001), and a time step of 5 s, satisfying the CFL stability condition (Courant et al. 1928); it is carried on for 17 h. We do not compute the interaction of the wavefield with very shallow bathymetry or initially dry land, but rather stop the computation at the 20-m isobath in the vicinity of coastlines. This procedure still allows the comparison, at a given site, of tsunamis emanating from neighboring but distant provinces. Note that the propagation of the wave landwards of our gauges, in depths $20 < h < 1000$ m, can slightly affect the waveshapes at the gauges themselves, as part of the shoaling process.

Figures 2 and 3 (using different palettes) show examples of the distribution of maximum amplitudes $\eta_{\max}$ over the Indian Ocean Basin. They constitute classical examples of the control of far-field tsunami amplitudes by a combination of directivity effects, with a maximum radiation in a direction perpendicular to the fault rupture (Ben-Menahem and Rosenman, 1972), and of focusing or defocusing by irregular bathymetry (Woods and Okal 1987; Satake 1988).

Directivity is especially prominent on Fig. 2, where the orientation of the main lobe rotates from mostly Westwards for model **S.I** (with a secondary lobe oriented Southwest) to exclusively Southwest in the other models, whose energy

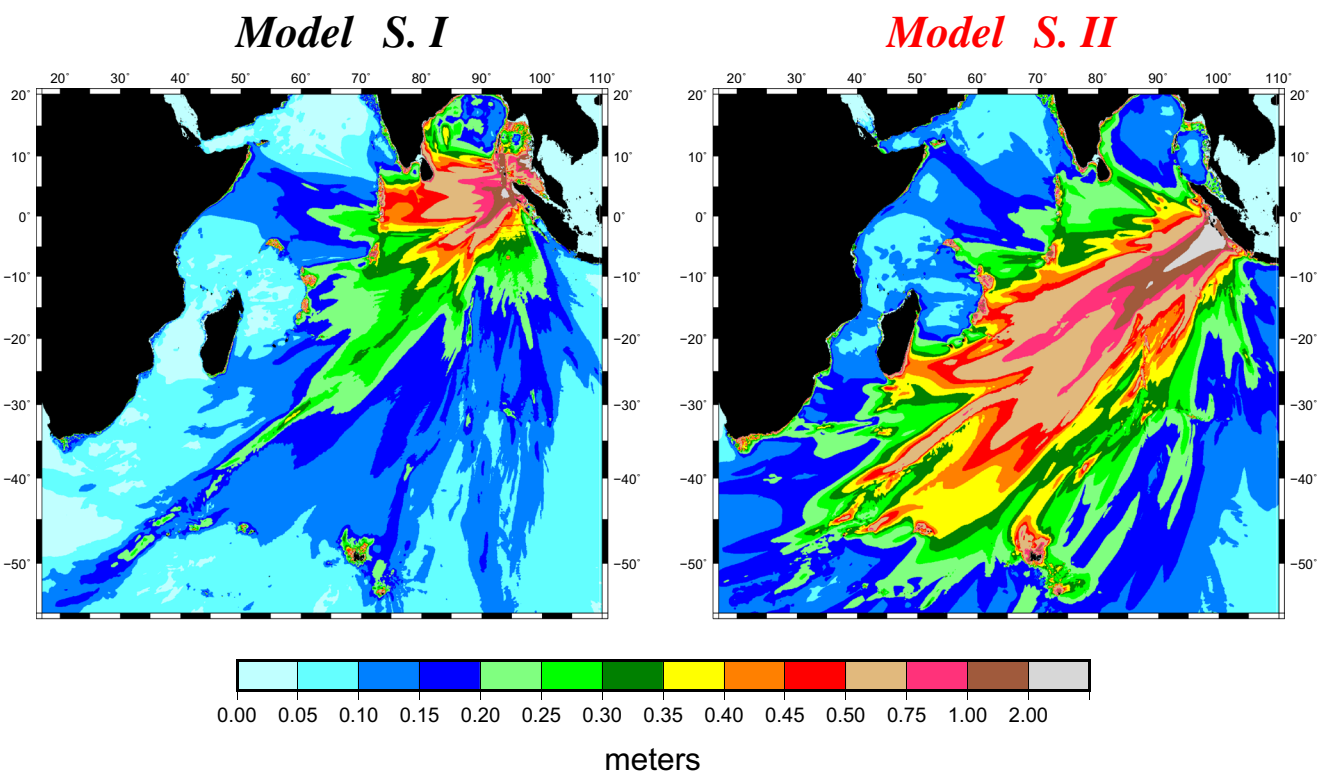

Fig. 2 Examples of basin-wide simulations in the case of Sumatra sources. Model **S.I** reproduces the 2004 Sumatra-Andaman event; Scenario **S.II** is a model the 1833 tsunami; scenario **S.IV** is a possible model of a future earthquake closing the Padang seismic gap; and scenario **S.V** includes a speculative rupture along the Southern part of the Sumatra Trench

is beamed towards largely empty parts of the basin (with the exception of isolated islands such as Amsterdam or Kerguelen), but could also affect the Mascarenes and Madagascar. Similarly, the Makran scenarios shown on Fig. 3 see most of their energy aimed at the Southern Indian Ocean Basin, with little if any refracted towards Africa. By contrast, the Western Coast of India is systematically illuminated by tsunami rays from the Makran sources (Burbidge et al. 2009).

The focusing effect of bathymetry is evident along the Southwest Indian Ocean Ridge which channeled the energy of the secondary 2004 lobe (model **S.I**) all the way into

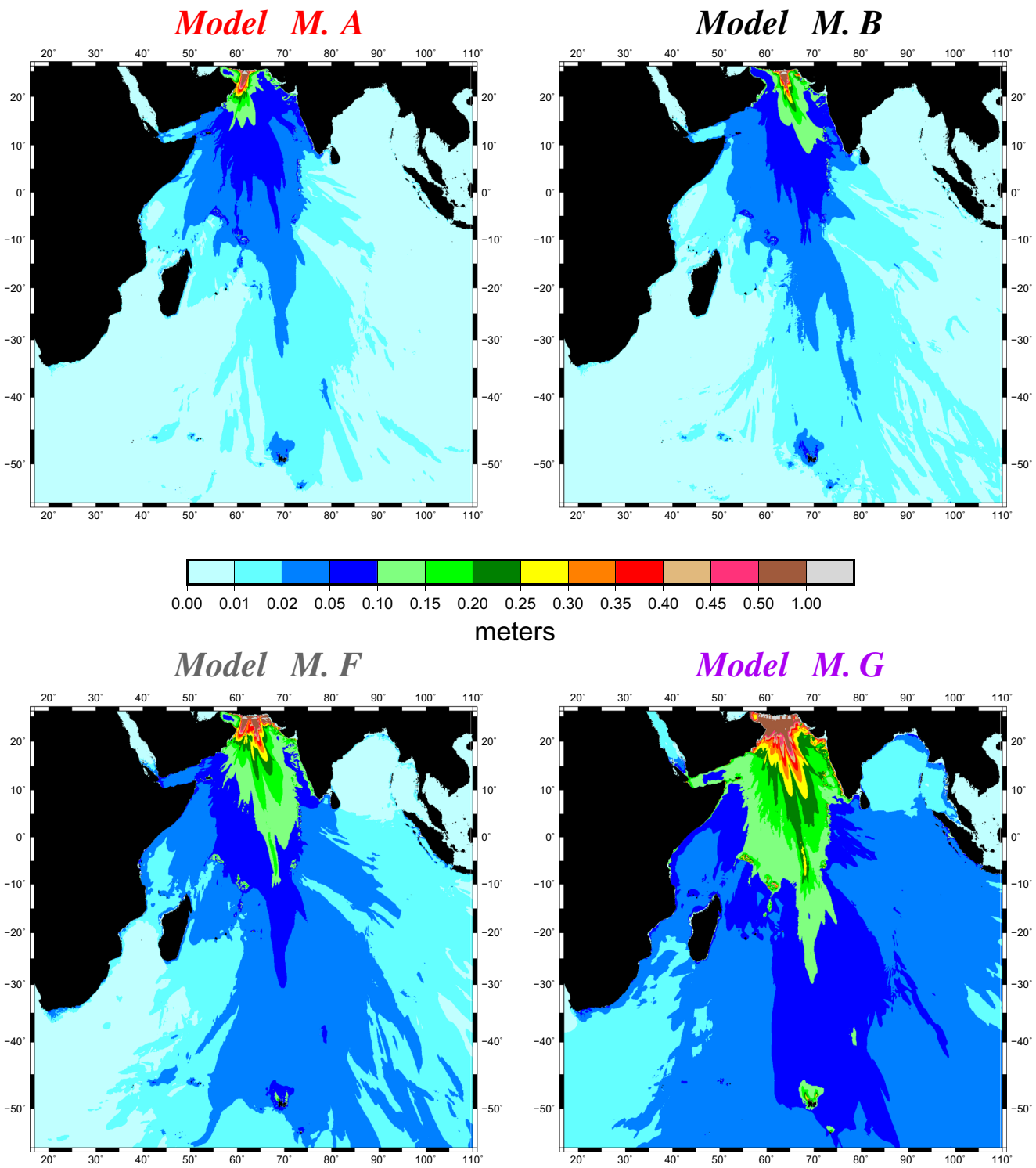

Fig. 3 Same as Fig. 2 for a selection of Makran simulations. Scenario **M.A** is a possible model of the 1851 event; scenario **M.B** is a model the 1945 tsunami; scenario **M.F** is a combination of the three blocks A, B, and C; and the speculative scenario **M.G** features a rupture propagating into the Western Makran

the Atlantic Ocean and even the Pacific through the Drake Passage (Titov et al. 2005), with similar focusing expected under scenarios **S.II** and **S.V**. Note also focusing by the Carlsberg Ridge, from South of the Maldives to Socotra and the Horn of Africa, under scenarios **S.II** and **S.V**, discussed in detail in the "Results: Sumatra; Figs. 2 and 4"

section. Finally, shallow bathymetry along the Laccadive-Maldives-Chagos chain acts as a barrier under scenario **S.I**, with sharply reduced amplitudes beyond it to the West; incidentally, in 2004, most of this energy was reflected back Eastwards, with relatively contained amplitudes in the Maldives (Fritz et al. 2006), whose structure as steep atolls leads to less efficient run-up than at shallow-dipping, Hawaiian-type islands, or continental slopes.

Results and discussion

Gauges

The locations of the 35 virtual gauges are given in Table 2 and mapped on Fig. 1. In order to prevent confusion with Paper I, while at the same time maximizing continuity in the gauge dataset, we re-index them starting at 101; this also allows to distinguish locations for those gauges whose site has been moved slightly to achieve commonality of water depths.

Figures 4a (Sumatra sources) and 5a (Makran sources) show the profiles of maximum amplitude at the gauges, as a function of their index. In Frames 4*b* and 5*b*, the same results are plotted relative to the reference event (2004, **S.I** in Sumatra; 1945, **M.B** in the Makran), using a logarithmic scale. The gray vertical-dotted lines separate groups of gauges whose location varies continuously with index, allowing a direct comparison of amplitude as the gauges are moved regularly along a shoreline or in an island group. As such, the dotted lines represent discontinuities in the distribution of gauges, across which the line plots have been interrupted. The first group consists of two gauges (101 and 102) located at the back of the Gulf of Aden, near the strategic ports of Djibouti and Aden. In the second group, the gauges move continuously along the Eastern coast of Arabia and Africa from Oman in the North (103) all the way to Port Elizabeth (118) in the South. The third group (119–123) features the four islands of the Comoro Archipelago and an additional gauge near the island of Nosy-Bé, off the Western coast of Madagascar, while the fourth one (124–126) covers its Eastern coast. The fifth group (127–130) samples the Seychelles and Mascarenes (Réunion, Mauritius and Rodrigues), while the last one (131–135) regroups the five islands of Amsterdam, St. Paul, Kerguelen and Crozet, part of the French Austral and Antarctic Lands, and the South African Prince Edward Islands.

Results: Sumatra; Figs. 2 and 4

We first focus on the coast of Africa, sampled continuously by Gauges 105–118, where maximum amplitudes are generally contained under 20 cm (with a couple of exceptions described below), and their lateral variations limited. When examining amplitudes relative to 2004 on Fig. 4b, we note a systematic increase from North to South, especially for models **S.II** and **S.V** which produce amplitudes larger than the 2004 event (model **S.I**), even though the moments of the parent earthquakes are smaller. As discussed above, this effect expresses directivity at the source (Ben-Menahem and Rosenman 1972), the major beam of radiation rotating to a Southwestern, as opposed to Western, azimuth. Additionally, local maxima in relative amplitudes, off Zanzibar (108) and Moma (113), correspond to minima under the 2004 scenarios, rather than to amplification in scenarios **S.II** or **S.V**.

Of particular interest is the recent discovery by Maselli et al. (2020) of sedimentological evidence of a flooding event about 1000 years ago, which led to the apparent eradication of a human settlement at the mouth of the Pangani River in Northern Tanzania at 5° S, i.e., between our gauges 107 (Mombasa, Kenya) and 108 (Zanzibar). Based on a detailed simulation of the 2004 and 1833 sources (including the response of the coastal site), Maselli et al. (2020) concluded that the weaker effects of the 2004 tsunami resulted from its occurrence at low tide. We note however that our model **S.II** would predict a slightly higher amplitude than in 2004 (by interpolation between gauges 107 and 109), reflecting the fact that Maselli et al.'s (2020) source for the 1833 earthquake is displaced South $\sim$ 200 km from our model **S.II** and would thus be more in line with our model **S.V**, which generally produces slightly lower amplitudes than **S.II** along that section of the coast.

Our simulations along the entire East African coast, confirmed by Maselli et al.'s (2020) observation at Pangani, constitute a major result, namely that the 2004 tsunami did not amount to a "worst-case scenario" from Kenya South, even though it led to significant casualties notably in Tanzania, where at least 12 people were confirmed dead, with reportedly more in the unsurveyed Southern part of the country (Okal et al. 2009), and probably in Mozambique where the tsunami was not surveyed. The only exception to this pattern would be Northern Somalia (105) where the large 2004 run-up amplitudes of 9 m reported by Fritz and Borrero (2006) resulted from particularly efficient Westward beaming at the source.

Contrary to this trend, and to the North, i.e., in Socotra (104) and in the Gulf of Aden (101 and 102), we find that models **S.II** and **S.V** predict significantly larger amplitudes than in 2004 (by a factor of nearly 3 for **S.II** at Djibouti (101). As shown on Fig. 2, this intriguing pattern can be explained by focusing along the Carlsberg Ridge, extending from the Maldives-Chagos passage ($\sim$3°S; 73°E) to Socotra and the Horn of Africa. This results in a continuous beam of energy further feeding into the the Gulf of Aden, the site of a similar ridge. Figure 2 suggests that the

Table 2 Locations of virtual gauges used in this study

Index		Latitude	Longitude	Location	Country
This study	Paper I	(° N)	(° E)		
101*		11.846	44.557	Djibouti	Djibouti
102		12.596	45.360	Aden	Yemen
103	1	17.475	56.500	Hallaniyah Is.	Oman
104	2	12.270	54.610	Socotra Is.	Yemen
105	3	9.100	51.205	Bandarbeyla	Somalia
106		1.866	45.625	Mogadishu	Somalia
107	5	−3.980	40.620	Mombasa	Kenya
108	6	−6.520	39.792	Zanzibar Is.	Tanzania
109		−10.440	40.745	Rovuma River	Tanzania/Mozambique
110		−10.790	40.863	Palma	Mozambique
111		−12.920	40.707	Pemba	Mozambique
112		−15.140	40.913	Nampula Province	Mozambique
113		−16.960	39.884	Moma	Mozambique
114		−19.000	37.380	Zambeze River	Mozambique
115	16	−19.960	36.620	Beira	Mozambique
116	17	−26.600	34.256	Maputo	Mozambique
117	18	−30.160	31.650	Durban	South Africa
118	19	−34.109	27.000	Port Elizabeth	South Africa
119	7	−11.450	43.555	Grande Comore	Comoros
120	8	−12.214	43.851	Moheli	Comoros
121	9	−12.048	44.510	Anjouan	Comoros
122	10	−12.560	45.233	Koungou, Mayotte	France
123		−12.227	48.363	Nosy−Bé	Madagascar (W)
124	11	−15.030	50.551	Antalaha	Madagascar (N)
125	12	−19.597	49.192	Mahanoro	Madagascar (C)
126	13	−23.991	47.700	Manantehina	Madagascar (S)
127	4	−4.490	56.451	Mahé	Seychelles
128	15	−20.814	55.521	Saint−Denis, Réunion	France
129		−20.109	57.443	Port−Louis	Mauritius
130	14	−19.640	63.590	Rodrigues	Mauritius
131		−37.796	77.619	Amsterdam Is.	France
132		−38.560	77.759	St. Paul Is.	France
133		−47.131	71.142	Kerguelen Is.	France
134		−46.314	52.000	Crozet Is.	France
135		−46.627	38.089	Prince Edward Is.	South Africa

* Exceptionally, Gauge 101 is located in water 856 m deep

conditions of refraction by the Maldives chain, and possibly diffraction at the Maldives-Chagos passage, result in a more concentrated beam in scenario **S.II** than for **S.I**, hence in a more consistent amplification. At any rate, these results are important, since they suggest that a 1833-type source would see higher run-up in Socotra than in 2004, when it reached 6 m and resulted in one casualty on the island (Fritz and Okal 2008). Also, they point out to model **S.II** as optimizing the penetration of the Gulf of Aden, a conclusion also reached in the case of Djibouti by Burbidge et al. (2009) from a probabilistic standpoint.

Farther South, another remarkable property is that the coastlines of Mozambique are only weakly sheltered by Madagascar, and the local minimum in amplitudes observed around Moma (110; ∼17°S), especially under Scenario **S.I**, remains about 2/3 of the values along unobstructed coastlines to the North, such as at Rovuma (105; ∼11°S). At the extreme Southern end of our profile, in Port Elizabeth (118), favorable beaming and focusing predict amplitudes as high as 2.5 times those in 2004, which inflicted significant damage in the harbor, and caused two casualties at a local beach (Rabinovich and Thomson 2007).

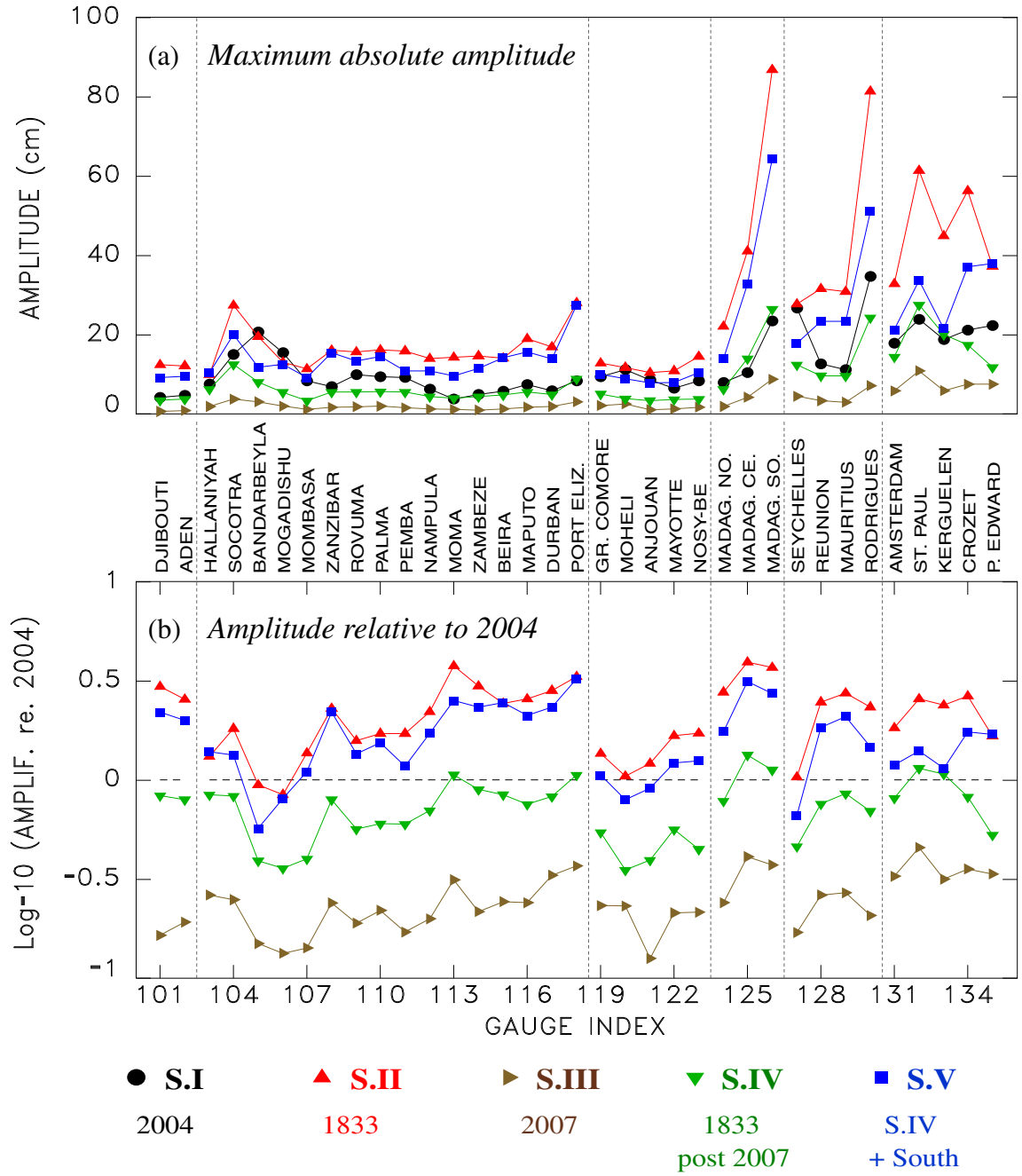

Fig. 4 Summary of Sumatra simulations at the 35 virtual gauges. **a** Maximum absolute amplitude recorded at each gauge, color-coded according to source model (see Table 1). **b** Amplitudes relative to 2004, plotted on a logarithmic scale. See text for discussion

By contrast, the various scenarios produce only limited amplitudes off the Comoro Islands, with only marginal amplification over the 2004 values in the case of model **S.II**. However, we recall that local run-up consistently reached 4 to 6.9 m along the Northern coast of Grande Comore (Okal et al. 2009), which leaves that island at significant risk under most future scenarios.

Our results are particularly critical in the case of the East coast of Madagascar, where all models show a regular increase in amplitude form North to South, already apparent on Fig. 2, and generally confirmed by the dataset of 2004 surveyed run-up values (Okal et al. 2006a). In this respect, Fig. 2 suggests that the Mascarene Plateau, a 1500-km continuous feature rising essentially to sea-level and linking the Seychelles to Mauritius, acts as a barrier effectively sheltering Northern Madagascar, while waves can reach its Southern coast by skirting the Mascarene Islands (Rodrigues, Mauritius and Réunion). When coupled

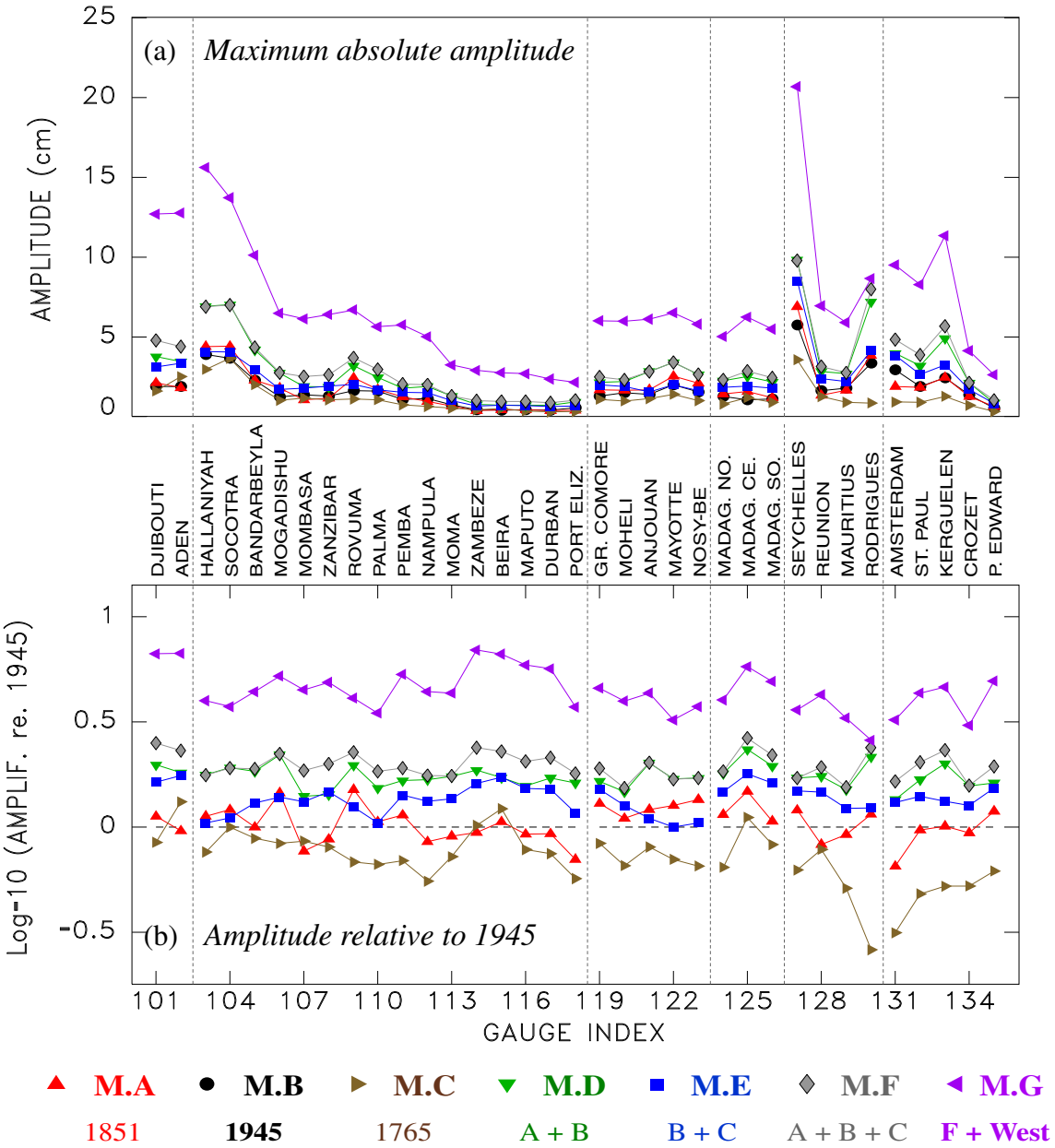

Fig. 5 Same as Fig. 4 in the case of the Makran simulations. Note the different vertical scale in (**a**). In (**b**), amplitudes are taken relative to the quantified event of 1945

with a favorable directivity under scenario **S.II** (and to a lesser extent, **S.V**), amplitudes could reach 3 to 4 times those of 2004, which resulted in run-up of up to 5.4 m at Betanty, at the extreme Southern tip of the island, and one casualty at Manafiafi, 35 km to the North (Okal et al. 2006a). Generally similar conclusions were also reached by Burbidge et al. (2009).

Regarding the fifth group, a more favorable directivity again leads to enhanced tsunami amplitudes under scenarios **S.II** and **S.V** in the Mascarene Islands (Réunion and Mauritius), where the 2004 tsunami ran up to 2.9 m. By contrast, the 2004 tsunami could constitute a worst-case scenario in the Seychelles (127), which clearly sit to the North of the directivity lobes of **S.II** and **S.V**. While the 1833 tsunami was observed in the Seychelles (Jackson et al. 2005), those reports are not quantitative.

Finally, for the last group of gauges considered, the scattered islands of the far Southern Ocean (131–135), model **S.II** once again represents the worst-case scenario, with amplitudes generally larger than in 2004 by a factor of more than 2, especially at St. Paul and Crozet. While the only population consists of rotating scientists numbering from 0 (St. Paul) to 100 (Kerguelen), for logistical reasons their settlements are usually established on coastal lowlands

where they could find themselves vulnerable to attack by tsunamis. For example, in the case of Crozet (134), the 2004 tsunami inundated more than 200 m inland, destroying the brooding grounds of a rookery of king penguins in the immediate vicinity of the research station at Baie du Marin (Viera et al. 2006), which could therefore be eradicated under scenario **S.II**.

Results: Makran; Figs. 3 and 5

When compared with the Sumatra scenarios, and with the exception of the speculative model **M.G**, simulations for the Makran sources yield generally much smaller amplitudes, not exceeding 10 cm; note the different palette on Fig. 3, and vertical scale on Fig. 5a. This is a combined reflection of the generally smaller size of the seismic sources, and of their orientation, which results in directivity lobes beaming SSE, away from Africa and its neighboring islands. For Makran sources, the reference event (**M.B**) consists of the well-documented, seismologically instrumented 1945 shock, whose tsunami has been both surveyed in the field (Okal et al. 2015; Anonymous 2015) and modeled (e.g., Heidarzadeh et al. 2008; Heidarzadeh and Satake 2015); note however that the 1945 earthquake triggered a significant submarine landslide, which should only marginally affect its tsunami in the far field.

The generally lower amplitudes simulated from the Makran sources also agree with Burbidge et al.'s (2009) conclusion that the Sumatra subduction zone is the main contributor to tsunami hazard for the overwhelming majority of the Indian Ocean coastlines.

Under this particular geometry, moving the source West (**M.A**) leaves the far-field pattern essentially unchanged, while moving it East (**M.C**) reduces amplitudes slightly, or even significantly at Rodrigues (130) and Amsterdam (131), these islands moving out of the main lobe of directivity. As expected, composite sources (**M.D, M.E, M.F**) feature values enhanced by an average factor of two, which could lead to significant run-up, especially in the Seychelles and Rodrigues. As expected, the speculative model **M.G**, which features an enhanced slip, further increases all far-field amplitudes, to an average of 4 times those of 2004, and as much as 6 times in the Gulf of Aden (101 and 102). It is the only model whose results approach those simulated for Sumatran sources. Their distribution along the coast of East Africa remains similar to those of smaller scenarios.

While the Comoros could see amplitudes enhanced to potential hazard levels comparable with those in 2004, the situation in Madagascar is not comparable with Sumatran scenarios, since it clearly sits outside the main lobe of directivity, and is further protected by the Northern branch of the Mascarene Plateau and the Seychelles. The latter location (127) features a large amplitude, which however fails to reach the level of the 2004 or 1833 Sumatran scenarios. Similarly, results at the Southern Island gauges are generally smaller than for Sumatran sources.

Conclusions

An enhanced update of our previous work in Paper I leads to the following conclusions:

- The distribution of off-shore tsunami amplitudes at a common water depth of 1000 m varies significantly with the location of mega-earthquakes along the Sumatra Trench, as a result of the combination of directivity effects and refraction by irregular bathymetry.
- Consequently, and despite its extreme moment (1.2×10^{30} dyn*cm), which may not be duplicated in future Sumatran large earthquakes, the 2004 Sumatra-Andaman event does not always constitute the worst-case scenario for tsunami hazard at various sites on the East African shoreline or its neighbor islands. We regard this as a crucial result, since the exceptional size of the 2004 event could give a false sense of security from a disastrous basin-wide tsunami during great earthquakes which may not match its seismic moment.
- Paramount among threatened shorelines is the case of Southern Madagascar, which could expect much larger waves than in 2004 (when they already reached 5 m run-up) in a repeat of the 1833 event, for which, incidentally, we lack reliable local reports.
- The whole Eastern coast of Africa would also face larger amplitudes from a source displaced South from the 2004 event, and increasingly so as the receiver is moved South, culminating in an amplification factor at Port Elizabeth of about 3 with respect to the 2004 scenario, when significant damage and two casualties occurred locally (Rabinovich and Thomson 2007).
- The Gulf of Aden could see large amplification (again by as much as a factor of 3), as a result of trapping of tsunami energy by the Carlsberg Ridge, during a repeat of the 1833 event.
- Remote islands of the Southern Indian Ocean are also prone to tsunami attacks at higher amplitudes than during the 2004 event, and despite their low population, their scientific bases could find themselves at risk.
- In general, tsunami hazard from large events in the Makran remains relatively low, due mainly to unfavorable directivity at the source, the only potential exception being the highly improbable model **M.G**, which could occasionally give rise to amplitudes comparable with those observed in 2004. Given the continuing level of speculation surrounding the nature of the plate convergence in the Western Makran, it is

clear that a program of multidisciplinary research is warranted in that region, including monitoring of sea-floor deformation through underwater geodesy, as well as paleo-tsunami investigations.

- Finally, a quantitative assessment of the effect of the 2004 tsunami in areas not covered by previous surveys is warranted, particularly in Southern Tanzania, and along the entire coast of Mozambique.

Acknowledgments We thank the conveners of the 2nd Conference of the Journal of Arabian Geosciences, Drs. Abdullah Al-Amri, Nabil Khelifi, and Mustapha Meghraoui, for their support. The paper was improved by the comments of three anonymous reviewers. Some figures were drafted using the GMT software (Wessel and Smith 1991).

Funding This research was supported at the University of Michigan by the National Science Foundation under Grant 1663769 of the PREEVENTS program.

References

Ambraseys NN, Melville CP (1982) A history of Persian earthquakes. Cambridge Univ Press, Cambridge

Ando M (1975) Source mechanism and tectonic significance of historical earthquakes along the Nankai Trough, Japan. Tectonophysics 27:119–140

Anonymous (2001) ETOPO2, Global 2 arc-minute ocean depth and land elevation from the US National Geophysical Data Center. NOAA, U.S. Dept Commerce, Washington, D.C

Anonymous (2005) United Nations Hyogo Declaration on Disaster Reduction, A/CONF.206/6, http://www.unhcr.org/refworld/docid/42b988b24.html

Anonymous (2015) Remembering the 1945 Makran tsunami. Intergov. Oceanog. Comm., UNESCO, Paris

Ben-Menahem A, Rosenman M (1972) Amplitude patterns of tsunami waves from submarine earthquakes. J Geophys Res 77:3097–3128

Bernard EN, Titov VV (2015) Evolution of tsunami warning systems and products. Phil Trans R Soc London Ser A 373:20140371, 14 p.

Borrero JC, Weiss R, Okal EA, Hidayat R, Suranto, Arcas D, Titov VV (2009) The tsunami of 2007 September 12, Bengkulu Province, Sumatra, Indonesia: Post-tsunami survey and numerical modeling. Geophys J Intl 178:180–194

Burbidge DR, Cummins PR, Mleczko R, Latief H, Mokhtari M, Natawidjaja D, Rajendran CP, Thomas C (2009) A probabilistic tsunami hazard assessment of the Indian Ocean nations. Geosci Australia Prof Opin 2009/11

Cisternas M, Atwater BF, Torrejón F, Sawai Y, Machuca G, Lagos M, Eipert A, Youlton C, Salgado I, Kamatabi T, Shishikura M, Rajendran CP, Malik JK, Rizal Y, Husni M (2005) Predecessors of the giant 1960 Chile earthquake. Nature 437:404–407

Courant R, Friedrichs K, Lewy H (1928) Über die partiellen Differenzengleichungen der mathematischen Physik. Math Ann 100:32–74

Davies G, Griffin J, Løvholt F, Glimsdal S, Harbitz V, Thio HK, Lorito S, Basili R, Selva J, Geist E, Baptista MA (2018) A global probabilistic tsunami hazard assessment from earthquake sources. Geol Soc London Spec Pub 456:219–244

Derakhti M, Dalrymple RA, Okal EA, Synolakis CE (2019) Temporal and topographic source effects in tsunami generation. J Geophys Res Oceans 124:5270–5288

Fritz HM, Borrero JC (2006) Somalia field survey after the December 2004 Indian Ocean tsunami. Earthquake Spectra 22:S219–S233

Fritz HM, Okal EA (2008) Socotra Island, Yemen: Field survey of the 2004 Indian Ocean tsunami. Nat Hazards 46:107–117

Fritz HM, Synolakis CE, McAdoo BG (2006) Maldives field survey after the December 2004 Indian Ocean tsunami. Earthquake Spectra 22:S137–S154

Godunov SK (1959) Finite difference methods for numerical computations of discontinuous solutions of the equations of fluid dynamics. Matematicheskiĭ Sbornik 47:271–295

Green G (1838) On the motion of waves in a variable canal of small depth and width. Trans Cambridge Philos Soc 6:457–462

Heidarzadeh M, Satake K (2015) New insights into the source of the Makran tsunami of 27 November 1945 from tsunami waveforms and coastal deformation data. Pure Appl Geophys 172:621–640

Heidarzadeh M, Pirooza MD, Zakerb NH, Yalçıner AC, Mokhtari M, Esmaeilye A (2008) Historical tsunami in the Makran Subduction Zone off the southern coasts of Iran and Pakistan and results of numerical modeling. Ocean Eng 35:774–786

Jackson LE, Barrie JV, Forbes DL, Shaw J, Mawson GK, Schmidt M (2005) Effects of the 26 December 2004 Indian Ocean tsunami in the Republic of Seychelles. Eos, Trans Amer Geophys Un 86(52):F6–F7 [abstract]

Jankaew K, Atwater BF, Sawai Y, Choowong M, Charoentitrat M, Martin MF, Prendergast A (2008) Medieval forewarning of the 2004 Indian Ocean tsunami in Thailand. Nature 455:1228–1231

Kelsey HM, Nelson AR, Hemphill-Haley E, Witter RC (2005) Tsunami history of an Oregon coastal lake reveals a 4600-yr record for great earthquakes on the Cascadia subduction zone. Geol Soc Amer Bull 117:1009–1032

Kukowski N, Schillhorn T, Flueh ER, Hurn K (2000) Newly identified strike-slip plate boundary in the Northeastern Arabian Sea. Geol 28:355–358

Mansinha L, Smylie DE (1971) The displacement fields of inclined faults. Bull Seismol Soc Amer 61:1433–1440

Maselli V, Oppo D, Moore AL, Gusman AR, Mtelela C, Iacopini D, Taviani M, Mjerna E, Mulaya E, Che M, Tomioka AL, Mshiu E, Ortiz JD (2020) A 1000-yr-old tsunami in the Indian Ocean points to greater risk for East Africa. Geology 48:808–813

McCloskey J, Lange D, Tilmann F, Nalbant SS, Bell AF, Natawidjaja DH, Rietbock A (2010) The September 2009, Padang earthquake. Nature Geosci 3:70–71

Mokhtari M, Fard IA, Hessami Kh (2008) Structural elements of the Makran region, Oman Sea and their potential relevance to tsunamigenesis. Nat Hazards 47:185–199

Musson RMW (2009) Subduction in the Western Makran: the historian's contribution. J Geol Soc London 166:387–391

Nanayama F, Satake K, Furukawa R, Shimokawa K, Atwater BF, Shigeno K, Yamaki S (2003) Unusually large earthquakes inferred from tsunami deposits along the Kuril trench. Nature 424:660–663

Natawidjaja D, Sieh K, Chlieh M, Galetzka J, Suwargadi B, Cheng H, Edwards RL, Avouac J-P, Ward S (2006) Source parameters of the great Sumatran earthquakes of 1797 and 1833 inferred from coral microatolls. J Geophys Res 111(B6):B06403, 37 p

Okal EA, Synolakis CE (2008) Far-field tsunami hazard from mega-thrust earthquakes in the Indian Ocean. Geophys J Intl 172:995–1015

Okal EA, Fritz HM, Raveloson R, Joelson G, Pančošková P, Rambolamanana G (2006a) Madagascar field survey after the December 2004 Indian Ocean tsunami. Earthquake Spectra 22:S263–S283

Okal EA, Fritz HM, Raad PE, Synolakis CE, Al-Shijbi Y, Al-Saifi M (2006b) Oman field survey after the December 2004 Indian Ocean tsunami. Earthquake Spectra 22:S203–S218

Okal EA, Sladen A, Okal EA-S (2006c) Rodrigues, Mauritius and Réunion Islands field survey after the December 2004 Indian Ocean tsunami. Earthquake Spectra 22:S241–S261

Okal EA, Fritz HM, Sladen A (2009) 2004 Sumatra tsunami surveys in the Comoro Islands and Tanzania and regional tsunami hazard from future Sumatra events. S Afr J Geol 112:343–358

Okal EA, Fritz HM, Hamzeh MA, Ghasemzadeh J (2015) Field survey of the 1945 Makran and 2004 Indian Ocean tsunamis in Baluchistan Iran. Pure Appl Geophys 172:3343–3356

Oldham RD (1893) A manual of the geology of India: stratigraphical and structural geology. Off. Superint. Gov. Printer, Calcutta.

Pendse CG (1948) The Mekran earthquake of the 28th November 1945. India Meteorol Dept Sci Notes 10:141–146

Rabinovich AB (1997) Spectral analysis of tsunami waves: separation of source and topography effects. J Geophys Res 102:12663–12676

Rabinovich AB, Thomson RE (2007) The 26 December 2004 Sumatra tsunami: analysis of tide gauge data from the world ocean; Part 1. Indian Ocean and South Africa. Pure Appl Geophys 164:261–308

Rajendran CP, Rajendran K, Machado T, Satyamurthy T, Aravazhi P, Jaiswal M (2006) Evidence of ancient sea surges at the Mamallapuram coast of India and implications for previous Indian Ocean tsunami events. Curr Sci 91:1242–1247

Rajendran CP, Rajendran K, Shah-Hosseini M, Naderi-Beni A, Nautiyal CM, Andrews R (2013) The hazard potential of the western segment of the Makran subduction zone, northern Arabian Sea. Nat Hazards 65:219–239

Reymond D, Okal EA (2000) Preliminary determination of focal mechanisms from the inversion of spectral amplitudes of mantle waves. Phys Earth Planet Inter 121:249–271

Saito T, Furumura T (2009) Three-dimensional tsunami generation simulation due to sea-bottom deformation and its interpretation based on the linear theory. Geophys J Intl 178:877–888

Satake K (1988) Effects of bathymetry on tsunami propagation: application of ray tracing to tsunamis. Pure Appl Geophys 126:27–36

Synolakis CE (2003) Tsunami and seiche. In: Chen W-F, Scawthron C (eds) Earthquake engineering handbook. CRC Press, Boca Raton, pp 9_1–9_90

Synolakis C, Bernard E, Titov V, Kânoğlu U, González F (2008) Validation and verification of tsunami numerical models. Pure Appl Geophys 165:2197–2228

Titov VV, Synolakis CE (1998) Numerical modeling of tidal wave runup. J Waterway Port Coast Oc Eng 124:157–171

Titov VV, Rabinovich AB, Mofjeld HO, Thomson RE, González FI (2005) The global reach of the 26 December 2004 Sumatra tsunami. Science 309:2045–2048

Titov VV, Kânoğlu U, Synolakis CE (2016) Development of MOST for real-time tsunami forecasting. J Waterway Port Coast Oc Eng 142(6):03116004, 16 p

Viera VM, Le Bohec C, Côté SD, Groscolas R (2006) Massive breeding failures following a tsunami in a colonial seabird. Polar Biol 29:713–716

Weiss R, Bahlburg H (2006) The coast of Kenya field survey after the December 2004 Indian Ocean tsunami. Earthquake Spectra 22:S235–S240

Wessel P, Smith WHF (1991) Free software helps map and display data. Eos, Trans Amer Un Geophys 72:441 and 445–446

White RS, Klitgord K (1976) Sediment deformation and plate tectonics in the Gulf of Oman. Earth Planet Sci Letts 32:199–209

Woods MT, Okal EA (1987) Effect of variable bathymetry on the amplitude of teleseismic tsunamis: a ray-tracing experiment. Geophys Res Letts 14:765–768

Zachariasen J, Sieh K, Taylor FW, Edwards RL, Hantoro WS (1999) Submergence and uplift associated with the giant 1833 Sumatran subduction earthquake: evidence from coral microatolls. J Geophys Res 104:895–919